Progression of Diet-Induced Diabetes in C57BL6J Mice Involves Functional Dissociation of Ca^{2+} Channels From Secretory Vesicles

Stephan C. Collins,[1] Michael B. Hoppa,[1] Jonathan N. Walker,[1] Stefan Amisten,[1] Fernando Abdulkader,[1,2] Martin Bengtsson,[1] Jane Fearnside,[3] Reshma Ramracheya,[1] Ayo A. Toye,[3] Quan Zhang,[1] Anne Clark,[1] Dominique Gauguier,[3] and Patrik Rorsman[1]

OBJECTIVE—The aim of the study was to elucidate the cellular mechanism underlying the suppression of glucose-induced insulin secretion in mice fed a high-fat diet (HFD) for 15 weeks.

RESEARCH DESIGN AND METHODS—C57BL6J mice were fed a HFD or a normal diet (ND) for 3 or 15 weeks. Plasma insulin and glucose levels in vivo were assessed by intraperitoneal glucose tolerance test. Insulin secretion in vitro was studied using static incubations and a perfused pancreas preparation. Membrane currents, electrical activity, and exocytosis were examined by patch-clamp technique measurements. Intracellular calcium concentration ($[Ca^{2+}]_i$) was measured by microfluorimetry. Total internal reflection fluorescence microscope (TIRFM) was used for optical imaging of exocytosis and submembrane depolarization-evoked $[Ca^{2+}]_i$. The functional data were complemented by analyses of histology and gene transcription.

RESULTS—After 15 weeks, but not 3 weeks, mice on HFD exhibited hyperglycemia and hypoinsulinemia. Pancreatic islet content and β-cell area increased 2- and 1.5-fold, respectively. These changes correlated with a 20–50% reduction of glucose-induced insulin secretion (normalized to insulin content). The latter effect was not associated with impaired electrical activity or $[Ca^{2+}]_i$ signaling. Single-cell capacitance and TIRFM measurements of exocytosis revealed a selective suppression (>70%) of exocytosis elicited by short (50 ms) depolarization, whereas the responses to longer depolarizations were (500 ms) less affected. The loss of rapid exocytosis correlated with dispersion of Ca^{2+} entry in HFD β-cells. No changes in gene transcription of key exocytotic protein were observed.

CONCLUSIONS—HFD results in reduced insulin secretion by causing the functional dissociation of voltage-gated Ca^{2+} entry from exocytosis. These observations suggest a novel explanation to the well-established link between obesity and diabetes. ***Diabetes*** **59:1192–1201, 2010**

Type 2 diabetes develops as a result of insulin resistance and β-cell failure (1). The link between obesity and insulin resistance is well established (2). Diabetes results when genetically predisposed individuals are incapable of compensating for the insulin resistance inherent to obesity with appropriate levels of insulin (3).

Longitudinal diet studies on islet function in vivo are best performed in experimental animals (4). When fed a high-fat diet (HFD), C57BL/6J mice develop glucose intolerance within 4 weeks (5–7). However, there is little information on the underlying mechanisms at the level of β-cell ion channel, electrical activity, Ca^{2+} homeostasis, and exocytosis.

We show here, in agreement with earlier in vivo (8,9) and in vitro (10,11) studies, that whereas short periods on HFD enhance glucose-induced insulin secretion (GIIS), long periods result in its diminution. The inhibition of insulin secretion was not associated with any changes in β-cell electrical activity or intracellular calcium concentration ($[Ca^{2+}]_i$) signaling that may explain the effect. We now demonstrate that the suppression of insulin secretion instead involves a selective inhibition of exocytosis in response to short (action potential–like) stimulation. These findings suggest that high-fat feeding inhibits insulin secretion by disrupting the tight association between voltage-dependent Ca^{2+} channels and the Ca^{2+} sensor of exocytosis.

RESEARCH DESIGN AND METHODS

Male C57BL/6J mice, without mutations in the NNT gene (12), were transferred to a 40% HFD (Special Diets Services, Witham, Essex, U.K.; composition given in supplementary Fig. 5, available in an online appendix at http://diabetes.diabetesjournals.org/cgi/content/full/db09-0791/DC1) at the age of 5 weeks as previously described (7). Age-matched control mice were maintained on a standard carbohydrate diet (ND; B&K Universal, Hull, U.K.). All mice were fed ad libitum and kept under a 12-h light/dark cycle. All procedures were carried out according to national and institutional guidelines. Plasma insulin was measured using an ELISA kit (Mercodia, Uppsala, Sweden).

Intraperitoneal glucose tolerance tests (IPGTTs) were performed as previously described (7). For intraperitoneal insulin tolerance tests, mice were fasted overnight (4:00 P.M. to 9:00 A.M.). Fasting glucose levels were established using a one-touch Accuchek system (Roche). For the insulin tolerance test, a solution of 0.15 units/kg insulin was administered intraperitoneally. Blood glucose was determined at 15, 30, and 75 min afterward.

Immunohistochemistry is described in the supplementary material. Briefly, pancreata from three mice were dissected and 10 sections separated by 200 μm were analyzed for β-cell–positive area.

Animals were killed by cervical dislocation after an overnight fast and islets were isolated as described previously (10). All experiments except those

From the [1]Oxford Centre for Diabetes, Endocrinology and Metabolism, University of Oxford, Churchill Hospital, Oxford, U.K.; the [2]Department of Physiology and Biophysics, Institute of Biomedical Sciences, University of São Paulo, São Paulo, Brazil; and [3]The Wellcome Trust Centre for Human Genetics, University of Oxford, Oxford, U.K.

Corresponding author: Stephan Collins, stephan.collins@drl.ox.ac.uk.

Received 26 May 2009 and accepted 28 January 2010. Published ahead of print at http://diabetes.diabetesjournals.org on 11 February 2010. DOI: 10.2337/db09-0791.

in Fig. 7, Fig. 8, and supplementary Fig. 6 were done on freshly isolated islets/tissues. Static and dynamic measurements of insulin release were performed using published methods (11,13). All samples were measured by a commercially available RIA kit (IDS Ltd Euro Diagnostica distributor, Tyne & Wear, U.K.). $[Ca^{2+}]_i$ in intact islets was assessed using a dual-wavelength detector (PTI Systems) using the indicator fura-2AM (11). ATP measurements were carried out on batches of 10 islets preincubated for 1 h in 300 μl RPMI medium containing 2 mg/ml BSA and 1 mmol/l glucose as described previously (11). ATP content was normalized to protein content (DC protein assay; Bio-Rad, Hercules, CA). Glucose-induced changes in whole-cell ATP-sensitive K^+ (K_{ATP}) conductance and membrane potential were monitored in intact islets using the perforated patch whole-cell technique (14). Ca^{2+} currents and exocytosis were measured in single β-cells, obtained by dissociation of islets in a Ca^{2+}-free medium, using the standard whole-cell technique and media as reported elsewhere (15).

The total internal reflection fluorescence microscopic (TIRFM) experiments were carried out on an inverted microscope (16). The low-affinity Ca^{2+} indicator Oregon Green 6F (10 μmol/l) was used for the spatially resolved measurements of Ca^{2+} influx (Fig. 8). Intracellular Ca^{2+} diffusion was restricted by inclusion of 10 mmol/l EGTA in the intracellular solution (Fig. 8*A*). The data were quantified by calculating the standard deviation (σ) and mean fluorescence (μ) for the entire cell footprint and expressed as coefficient of variation (CV; i.e., σ/μ). Vesicles undergoing exocytosis were detected as the rapid brightening and dispersion punctuate spots of the fluorescent islet amyloid polypeptide (IAPP)-mCherry peptide cargo (17). The rate of exocytosis was normalized to the number of docked vesicles (number of granules released divided by number of visible granules).

Photorelease of "caged" Ca^{2+}" was initiated using a JML-C2 flashlamp (Rapp Optoelektronik, Hamburg, Germany). The pipette solution consisted of (mmol/l) 110 K-glutamate, 10 KCl, 20 NaCl, 1 $MgCl_2$, 25 HEPES (pH 7.1 with KOH), 3 MgATP, 0.1 cAMP, 3 NP-EGTA (Synaptic Systems, Goettingen, Germany), and 2 $CaCl_2$. The Ca^{2+} indicator Fluo-4 was included in this medium at a concentration of 0.05 mmol/l.

All experiments involving islets were done on the same day as isolation, whereas experiments performed on dispersed cells were performed the next day (after 12–24 h) or after 48 h, when viral infection was needed (Fig. 7*F*).

Statistical analyses were performed using Origin 8 (OriginLab, Bucks, U.K.) and SPSS. Data are presented as mean ± SEM when data are normally distributed. Statistical significances were evaluated by two-tailed Student *t* test.

RESULTS

High-fat feeding results in increased body weight, glucose intolerance, and insulin resistance. Mice fed the HFD for 3 weeks were hyperglycemic and exhibited impaired glucose tolerance after an intraperitoneal glucose load (Fig. 1*A*). However, insulin secretion in response to the glucose challenge was normal (Fig. 1*B*). Mice fed the HFD for 15 weeks exhibited marked basal hyperglycemia and impaired glucose tolerance 30 and 75 min after the glucose challenge (Fig. 1*C*). This correlated with increased basal plasma insulin and reduced first-phase insulin secretion (measured 15 min after the glucose challenge), whereas the second-phase secretion (measured between 30 and 75 min; Fig. 1*D*) was improved. The HFD mice had a 20% increase in body weight after 15 weeks, from 35 ± 1 to 42 ± 1 g ($P < 0.05$), and were insulin resistant. Whereas insulin reduced plasma glucose to ~2.5 mmol/l in ND mice, it remained >4 mmol/l 75 min after insulin injection in HFD mice (Fig. 1*E*).

Insulin secretion in vitro is improved by short-term HFD exposure and impaired in the longer term. Insulin content was identical in islets from mice fed ND and HFD for 3 weeks (Fig. 2*A*). Basal insulin secretion (2–6 mmol/l glucose) was twofold higher in HFD islets than in ND islets (Fig. 2*B*). In both ND and HFD islets, elevation of glucose to 12 and 20 mmol/l stimulated insulin secretion ~3- and ~4.2-fold (relative 6 mmol/l), respectively.

After 15 weeks, islet insulin content was ~15% higher in HFD islets than in control islets (Fig. 2*C*). In ND (but not in HFD) islets, 6 mmol/l glucose stimulated insulin secretion 1.7-fold above that seen at 2 mmol/l glucose (from 0.07 to 0.13%; Fig. 2*D*, *inset*). Insulin secretion elicited by 12–20 mmol/l glucose or 0.2 mmol/l tolbutamide was reduced by 25–30% in islets from mice on the HFD (Fig. 2*D* and *E*); no difference in ND and HFD islets was detected when insulin secretion was evoked by high extracellular K^+ (70 mmol/l in the presence of 20 mmol/l glucose; Fig. 2*E*).

Effects of long-term HFD on first- and second-phase insulin secretion. Perfused pancreata from ND mice displayed an ~100-fold increase in insulin secretion when stimulated with 20 mmol/l glucose (Fig. 3*A*). Insulin secretion (normalized to insulin content) was strongly reduced in mice fed the HFD for 15 weeks with first and second phase being equally suppressed (57 and 61%, respectively). Total pancreatic insulin content was twice as high in HFD mice as in ND mice (Fig. 3*B*).

High-fat feeding has little effect on $[Ca^{2+}]_i$. After 15 weeks on ND and HFD, glucose exerted a dual effect on $[Ca^{2+}]_i$ in mouse islets: after an initial lowering, glucose increased $[Ca^{2+}]_i$ (Fig. 4*A* and *B*). In the presence of 12 mmol/l glucose, $[Ca^{2+}]_i$ oscillated with a period that averaged 14 and 11 s in HFD and ND islets, respectively (Fig. 4, insets; $P = 0.08$). As has been reported previously, these rapid oscillations were sometimes superimposed on a slower rhythm (18). Peak and average steady-state glucose-induced increases in $[Ca^{2+}]_i$ were similar in ND and HFD islets. $[Ca^{2+}]_i$ measured in the presence of 0.1 mmol/l tolbutamide was also not different between ND and HFD islets (not shown). Finally, exposing islets to 70 mmol/l extracellular K^+, in presence of 2 mmol/l glucose, produced identical increases in $[Ca^{2+}]_i$ in ND and HFD islets (supplementary Fig. 1).

In mice fed the ND and HFD for 3 weeks, $[Ca^{2+}]_i$ changes elicited by glucose and tolbutamide were, apart from a higher initial peak in HFD islets after addition of glucose, almost identical (supplementary Fig. 2).

Islet β-cell mass is increased by HFD exposure after 15 weeks but β-cells are structurally intact. Immunohistochemical analyses of pancreatic sections revealed no difference in β-cell area and average islet size between ND and HFD mice at 3 weeks after diet introduction (Fig. 5*A*). At 15 weeks, the average islet size and the total β-cell area were 1.2- and 1.5-fold higher in HFD than in ND mice (Fig. 5*B*) but the number of islets was not affected and averaged 1.13 ± 0.1 and 1.02 ± 0.1 islet/mm^2 in ND and HFD pancreata, respectively. Total islet protein content was 1.2-fold higher in HFD than in ND islets ($P = 0.04$; not shown).

Electron microscopy revealed no alterations of β-cell ultrastructure in ND and HFD islets (supplementary Fig. 3*A–D*). The absence of degranulation is consistent with the finding that islet insulin content was not reduced by high-fat feeding (compared with Fig. 2*D*).

Effects of HFD on whole-cell K_{ATP} conductance. Because islet function and insulin secretion were not impaired after 3 weeks on the HFD, the remainder of the study focused on the consequences of 15 weeks on HFD.

In both ND and HFD β-cells, the resting whole-cell conductance, principally reflecting K_{ATP} channel activity, was maximally inhibited already in the presence of 12 mmol/l glucose (supplementary Fig. 4*A*). No further reduction of whole-cell conductance was observed at 20 mmol/l glucose. The ability of glucose to block K_{ATP} channel activity was independent of diet type.

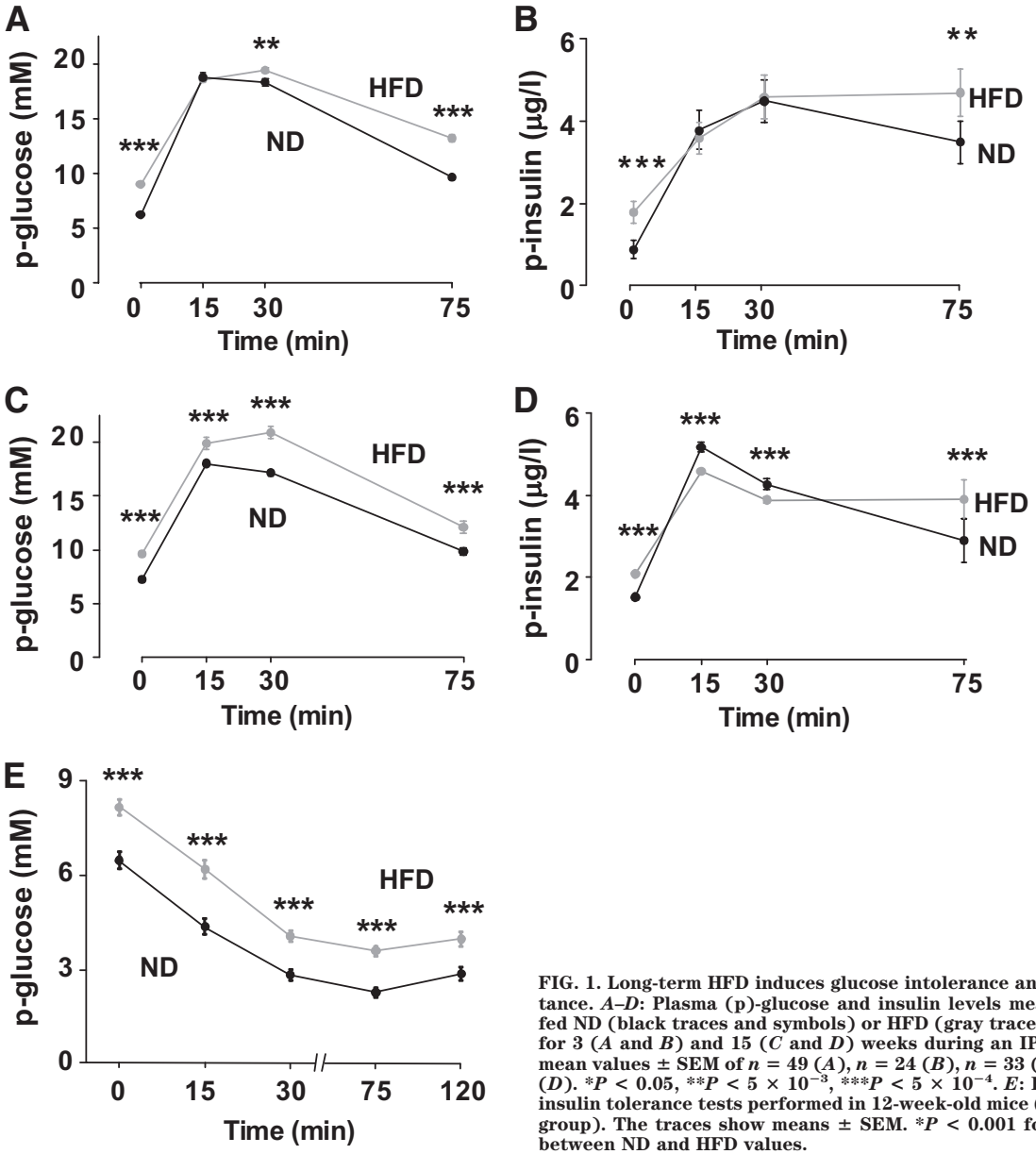

FIG. 1. Long-term HFD induces glucose intolerance and insulin resistance. *A–D*: Plasma (p)-glucose and insulin levels measured in mice fed ND (black traces and symbols) or HFD (gray traces and symbols) for 3 (*A* and *B*) and 15 (*C* and *D*) weeks during an IPGTT. Data are mean values ± SEM of $n = 49$ (*A*), $n = 24$ (*B*), $n = 33$ (*C*), and $n = 14$ (*D*). *$P < 0.05$, **$P < 5 \times 10^{-3}$, ***$P < 5 \times 10^{-4}$. *E*: Intraperitoneal insulin tolerance tests performed in 12-week-old mice ($n = 23$ in each group). The traces show means ± SEM. *$P < 0.001$ for comparisons between ND and HFD values.

β-Cell electrical activity is marginally increased, but ATP levels are not affected by HFD. Insulin secretion is tightly linked to β-cell electrical activity (19). The membrane potential of β-cells exposed to 2 mmol/l glucose was identical in ND and HFD β-cells within freshly isolated islets and averaged −66 ± 2 and −67 ± 2 mV, respectively. Upon stimulation with 12 mmol/l glucose, the β-cells depolarized to −40 ± 3 in ND islets and to −39 ± 2 mV in HFD islets. In both ND and HFD islets, membrane depolarization was associated with the initiation of oscillatory electrical activity consisting of bursts of action potentials superimposed on depolarized plateau separated by repolarized silent intervals (Fig. 6*A* and *B*). The fraction active phase at 12 mmol/l glucose averaged 65–70% in both ND and HFD islets. Both ND and HFD islets responded with increased electrical activity when exposed to 20 mmol/l glucose. Under the latter conditions, the inclusion of tolbutamide in the perfusion medium exerted no additional stimulatory effect.

Consistent with the lack of obvious changes in $[Ca^{2+}]_i$ handling and electrical activity, ATP production (normalized to islet protein) was unaltered in HFD islets (supplementary Fig. 4*B*).

Abnormal exocytotic pattern after 15 weeks on HFD. We compared the exocytotic capacity of β-cells from mice fed the ND and the HFD for 15 weeks. Exocytosis (monitored as increases in membrane capacitance) was evoked by a train of twenty 50-ms (Fig. 7*A*) or ten 500-ms (Fig. 7*C*) depolarizations from −70 mV to 0 mV. In Fig. 7*B* the cumulative change in ΔC_m ($\sum \Delta C_m$) is displayed against the cumulative charge of the Ca^{2+} currents ($\sum Q$) during the train of the 50-ms pulses. In β-cells from ND and HFD mice, the slopes of the relationship were 3.4 ± 0.8 fFarad/pCoulomb (fF/pC) and 0.9 ± 0.4 fF/pC ($P < 0.006$), respectively. Figure 7*D* compares the exocytotic responses in ND and HFD β-cells evoked by the individual 500-ms depolarizations during the pulse train. Exocytosis evoked by the first 500-ms depolarization tended to be slightly inhibited (by ~35%; $P < 0.06$) in HFD β-cells, but the responses during the rest of the trains were not affected. The total responses evoked by the trains of 50

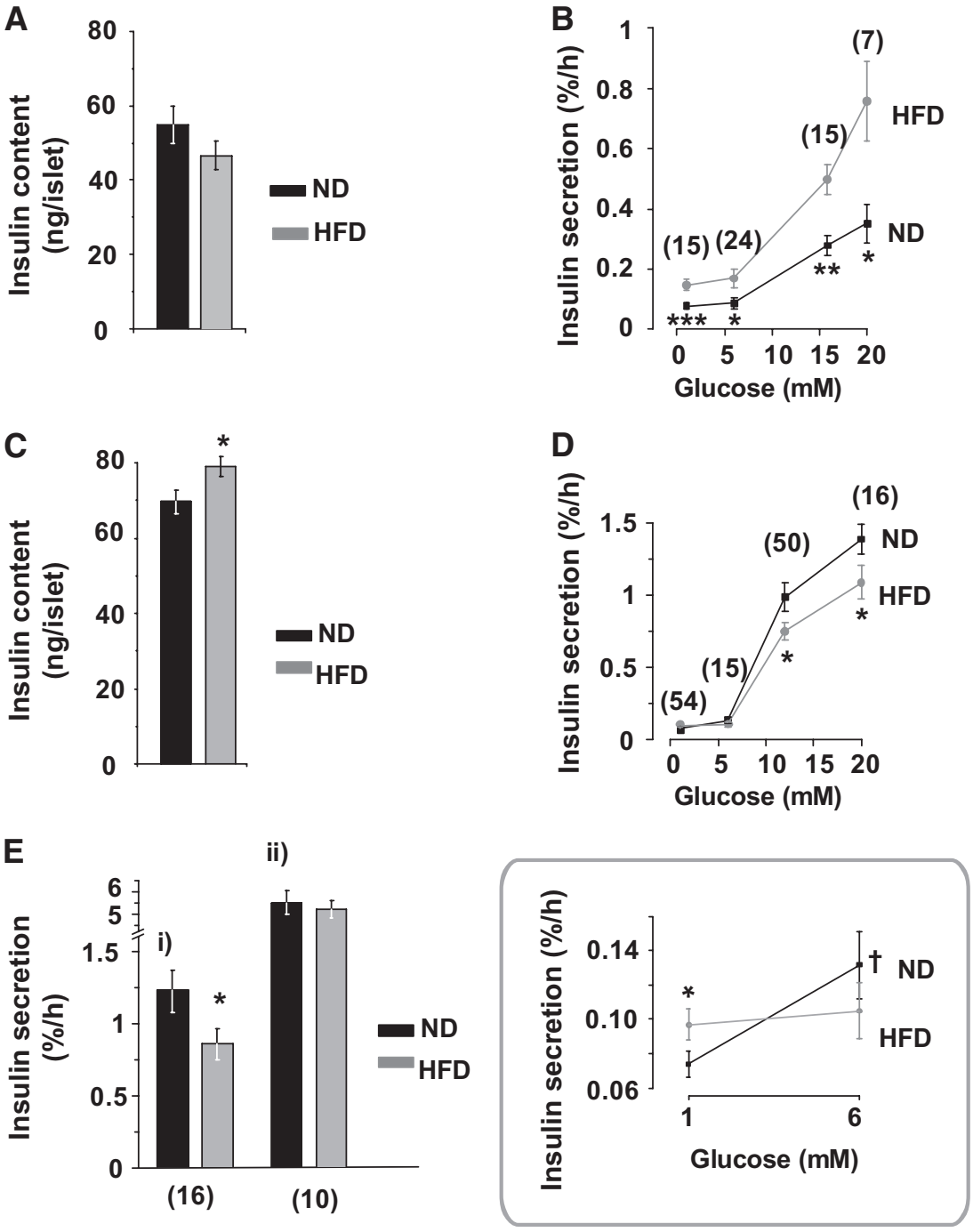

FIG. 2. Effects of HFD on GIIS in vitro. *A–E*: Insulin content (*A* and *C*) and insulin secretion (*B*, *D*, and *E*) in ND (black) and HFD (gray) islets. Data are from mice fed ND or HFD for 3 (*A* and *B*) and 15 (*C–E*) weeks. *B* and *D*: The islets were challenged with glucose at the indicated concentrations. *Ei*: Islets were stimulated by 0.2 mmol/l tolbutamide in the presence of 12 mmol/l glucose. *Eii*: Islets were stimulated by 70 mmol/l KCl in the presence of 20 mmol/l glucose. *D inset*: The data highlighted within the box compare insulin secretion at 1 and 6 mmol/l in ND and HFD islets. The number below each point represents the minimum number of cases in that group. At least four different animals were used in each group. Data are mean values ± SEM. *$P < 0.05$, **$P < 0.005$, ***$P < 0.0005$ for differences between ND and HFD. †$P < 0.05$ indicates difference between 6 and 1 mmol/l glucose. Numbers in parentheses in (*B*, *D*, and *E*) are number of experiments performed.

ms and 500 ms in ND and HFD β-cells are summarized in Fig. 7*E*. It is evident that HFD selectively inhibits exocytosis elicited by the short pulses.

We also monitored exocytosis optically in β-cells from ND and HFD mice by TIRF imaging. To visualize the granules, cells were infected with IAPP-mCherry. The granule density in the footprint of the cells averaged $0.67 \pm 0.06\ \mu m^{-2}$ ($n = 5$) and $0.72 \pm 0.05\ \mu m^{-2}$ ($n = 7$) in ND and HFD β-cells, respectively. The surface area of the β-cell (estimated from the cell capacitance and using a specific membrane capacitance of $9\ fF\mu m^{-2}$) used in these experiments averaged $682 \pm 63\ \mu m^2$ (ND) and $785 \pm 055\ \mu m^2$ (HFD). From these values, we estimated that the number of near-membrane granules was ~500 for both ND and HFD β-cells, similar to the number of docked granules determined by electron microscopy (20). Exocytosis was elicited by a 1-s depolarization to 0 mV (Fig. 7*D*). The depolarization triggered the release of some of the docked

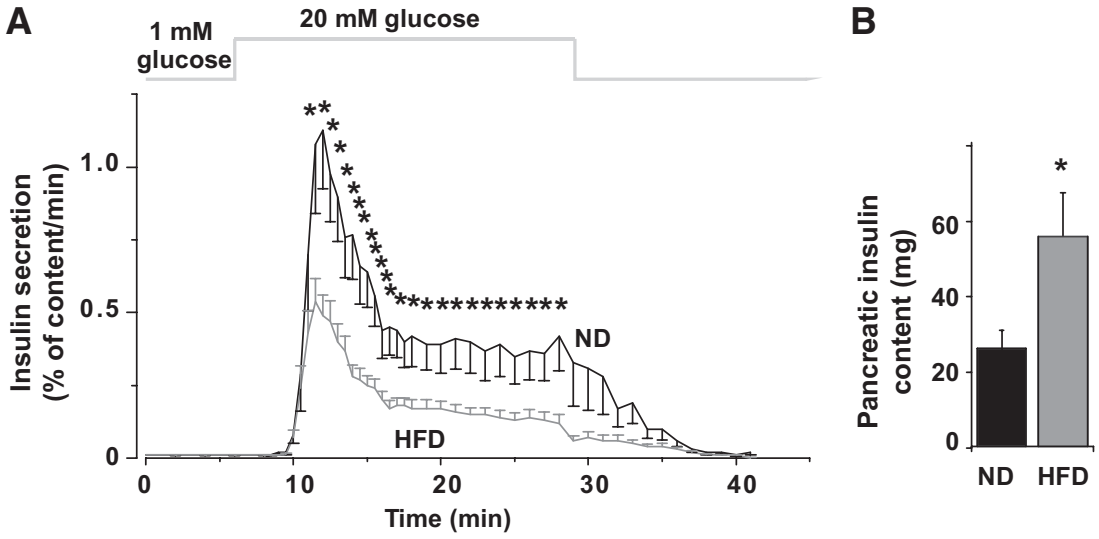

FIG. 3. HFD reduces first- and second-phase release equally. GIIS in perfused pancreata from control (black) and HFD (gray) mice (*A*) at 15 weeks. The rates of insulin secretion are given as mean values ± SEM and are normalized to pancreatic insulin content. *B*: Total pancreatic insulin content in ND (black) and HFD (gray) mice. **P* < 0.05 vs. control (*n* > 15 mice in each group).

granules (no newcomers [21] were released during this period). We found that cargo release was significantly reduced during the first 600 ms of the 1-s–long depolarization in the HFD cells.

Dispersion of local $[Ca^{2+}]_i$ transients reduces the chances of vesicle fusion. Exocytosis in β-cells is dependent on a tight association of Ca^{2+} channels to secretory granules (22). We performed spatially resolved measurements of the submembrane $[Ca^{2+}]_i$ by TIRFM (Fig. 7*E* and *F*). With low intracellular buffering (0.5 mmol/l EGTA), even depolarizations as short as 50 ms evoke widespread increases in $[Ca^{2+}]_i$ across the entire footprint of the β-cell and the CV was ~0.70 (Fig. 8*Ai*). It can be noted that the increase in $[Ca^{2+}]_i$ is restricted to the depolarization and that it promptly returned toward baseline upon repolarization (*vertical dotted lines* in Fig. 8*A*). As the depolarization was extended to 500 ms, the increase in $[Ca^{2+}]_i$ became more uniform and CV was accordingly reduced. When intracellular Ca^{2+} diffusion was restricted by inclusion of 10 mmol/l EGTA (Fig. 8*Aii*) or 0.5 mmol/l BAPTA (1,2-bis(o-aminophenoxy)ethane-*N*,*N*,*N*′,*N*′-tetraacetic acid; Fig. 8*Aiii*), Ca^{2+} entry was confined to discrete areas and

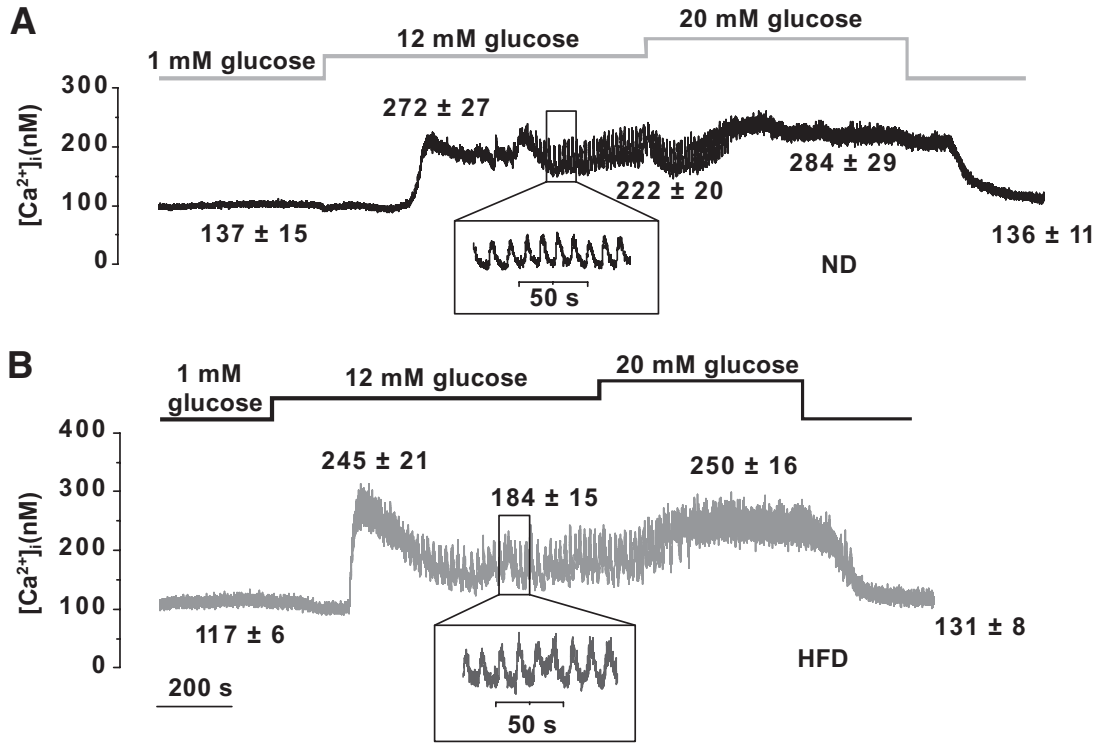

FIG. 4. Effects of HFD on $[Ca^{2+}]_i$. Glucose- and tolbutamide-evoked changes in $[Ca^{2+}]_i$ in islets from mice fed the ND (*A*) and HFD (*B*) for 15 weeks. Representative traces are shown for each group. Values given above the traces are means ± SEM (*n* > 13 islets from seven mice). **P* < 0.05 for comparisons of $[Ca^{2+}]_i$ under the respective conditions in ND and HFD islets.

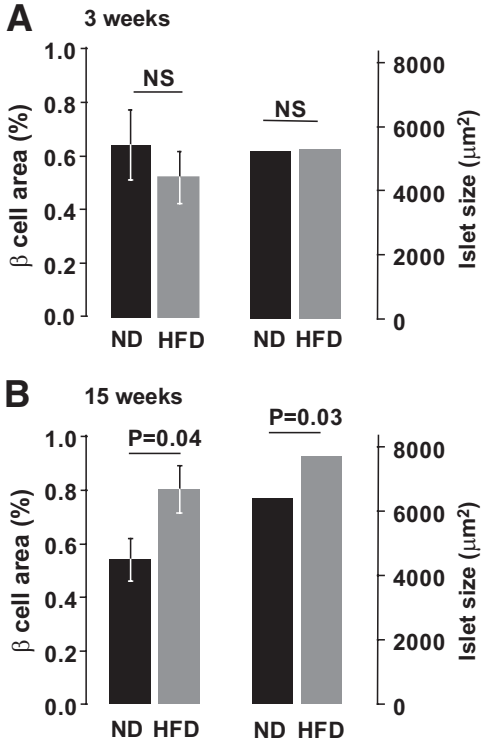

FIG. 5. Effects of HFD on β-Cell area. β-Cell surface area ratio to pancreatic surface area (*left*) and mean islet size (*right*) after 3 (*A*) or 15 (*B*) weeks on ND and HFD. Up to 24 sections taken from three mice were analyzed for each group. Data are mean values ± SEM. In the case of average islet size, significance levels (indicated above histograms) were calculated on transformed data (logarithm).

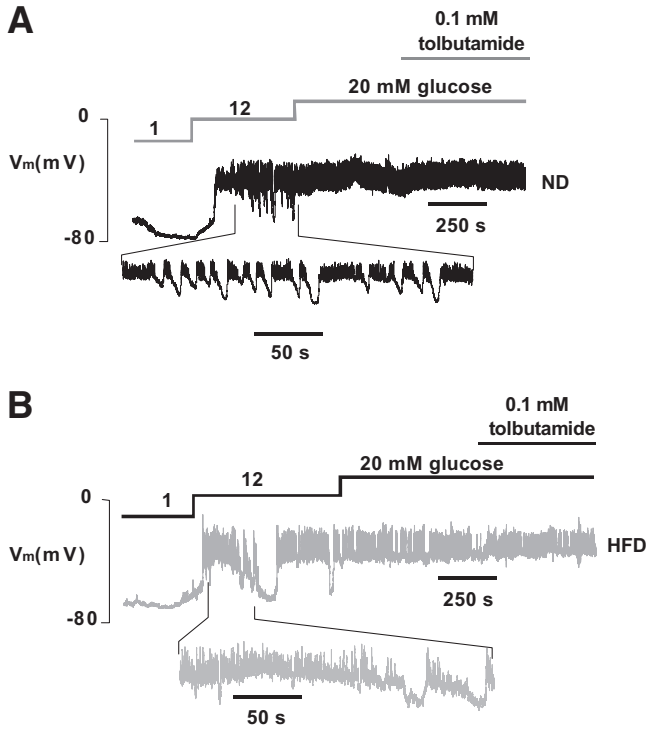

FIG. 6. Effects of 15 weeks of HFD on β-Cell electrical activity. *A* and *B*: Representative membrane potential (V_m) recordings from β-cells in intact ND (*A*) and HFD (*B*) islets (n = 7 islets in both groups, from four different animals). Segments of the records obtained at 12 mmol/l glucose (taken as indicated) are shown on an expanded time base below for both ND and HFD islets.

the CVs increased 1.6- to 1.9-fold. The $[Ca^{2+}]_i$ increases evoked by 50-ms depolarizations from −70 to 0 mV were less concentrated in HFD than in ND β-cells and the CV was reduced by ~14% (Fig. 8*B*). The CV of the prestimulatory fluorescence was also analyzed (to assess differences in factors such as dye loading and cell adherence) but no differences were observed (0.18 ± 0.01 vs. 0.16 ± 0.01 in ND and HFD β-cells, respectively). The magnitude of the $[Ca^{2+}]_i$ transients was unaffected and the integrated Ca^{2+} currents were −9.1 ± 1.4 and −9.9 ± 1.8 pC in ND and HFD β-cells, respectively. In Fig. 7*F*, we noted that hardly any granules underwent exocytosis during the first 100–200 ms. This is at variance with our previous observations made in β-cells isolated from NMRI mice (16). We measured exocytosis in C57BL6J β-cells in response to an instant and uniform elevation of $[Ca^{2+}]_i$ produced by photoliberation of Ca^{2+} (Fig. 8*C*). The estimated delay (derived by linear back-extrapolation of the capacitance increase to the baseline) averaged 209 ± 70 ms (n = 7).

Gene transcription not affected in HFD islets. We compared the mRNA levels of a panel of 22 selected genes in HFD and ND islets (supplementary Table 1). No differences in gene expression were observed.

DISCUSSION

Early effects of HFD: partial but insufficient β-cell compensation. After 3 weeks, both basal plasma glucose and glycemic values during the IPGTT were elevated in HFD mice. These observation are in agreement with the report that 2 weeks on a HFD results in improved GIIS in Sprague-Dawley rats (23).

The stimulation of insulin secretion observed after 3 weeks on the HFD was not secondary to enhanced elevation of $[Ca^{2+}]_i$, and the responses in ND and HFD islets were virtually superimposable. Previous studies in vitro have indicated that the acute stimulatory effect of free fatty acids (FFAs) on insulin secretion involves increased whole-cell peak Ca^{2+} currents (10) and/or inhibition of the voltage-gated K^+ (K_v) current that underlies action potential repolarization (24); both effects would be expected to elevate $[Ca^{2+}]_i$. The lack of any major increase in the glucose-induced elevation of $[Ca^{2+}]_i$ argues that such effects contribute little to the stimulation of insulin secretion seen in vivo. The acute stimulatory effects of the FFA palmitate in vitro are principally attributable to enhanced exocytosis (10). The observation that insulin secretion was enhanced in the face of an unchanged $[Ca^{2+}]_i$ indicates that short-term HFD likewise leads to enhanced exocytosis.

Long-term effects of HFD: impaired β-cell function. Our data confirm the adverse effects of long-term HFD on insulin secretion previously reported by others (25–27). In agreement with earlier observations (27), we observed a 1.5- and 2-fold increase in pancreatic β-cell area and insulin content, respectively. Mice on the HFD developed impaired glucose tolerance as a result of insulin resistance. Insulin secretion was apparently insufficient to meet the biological demand—again, in agreement with previous reports (28,29).

What is the cellular mechanism leading to reduced insulin secretion? The similar reduction in glucose- and tolbutamide-induced insulin secretion in the HFD group (Fig. 2*D* and *E*) suggests that the suppression of insulin secretion does not result from impaired glucose sensing.

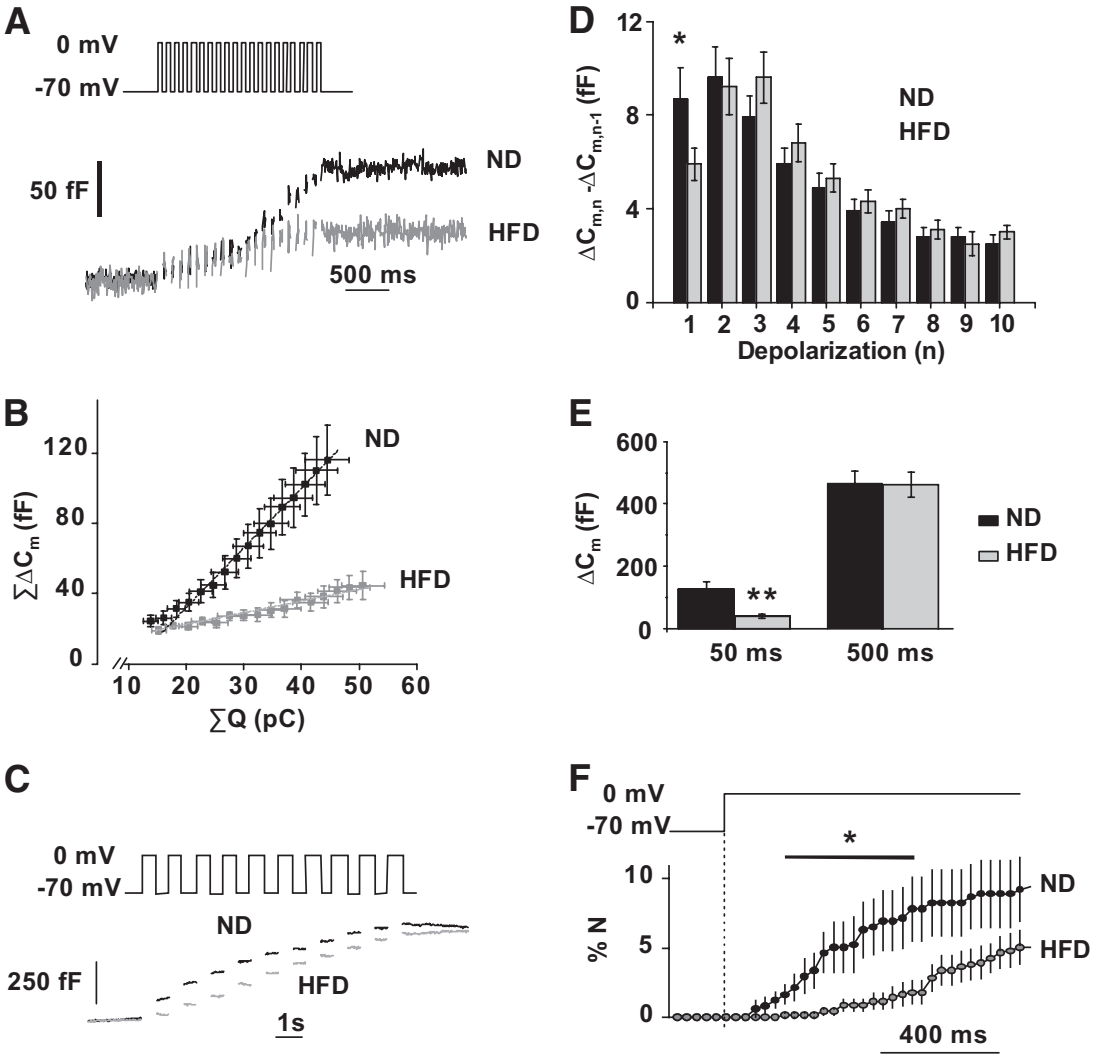

FIG. 7. A 15-week HFD treatment inhibits depolarization-evoked exocytosis. *A*: Representative recordings of exocytosis during a train of 50-ms (10 Hz) depolarizations from −70 mV to 0 mV in ND (black) and HFD (gray) β-cells. *B*: Relationship between integrated current charge ($\sum Q$) and changes in membrane capacitance ($\sum \Delta C_m$) during the train of twenty 50-ms depolarizations (10 Hz). The responses during the four first depolarizations (not associated with exocytosis) are not shown. The lines superimposed on the data points indicate the slopes of the relationships. *C*: Representative increases in cell capacitance evoked by a train of ten 500-ms (1 Hz) depolarizations from −70 mV to 0 mV in ND (black) and HFD (gray) β-cells. *D*: Increase in cell capacitance for each pulse during the train of 500-ms depolarizations in ND (black) and HFD (gray) β-cells. Mean values ± SEM for 75 (ND) and 61 (HFD) cells. *$P < 0.06$. *E*: Total capacitance increments (in fF) following the train of 50-ms (black) and 500-ms (gray) pulses. Data are means ± SEM for at least 61–75 β-cells from six animals from each group in the long pulses experiment and for at least 23 β-cells from three animals from each group in the short pulses experiment. **$P < 0.005$. *F*: Average rates of optically measured release of vesicles by discharge of fluorescent IAPP-mCherry cargo during a 1,000-ms membrane depolarization to 0 mV. Data are means ± SEM for 5 and 6 cells from two animals in each group for both ND (black) and HFD (gray) β-cells. *$P < 0.05$.

Indeed, both glucose-induced $[Ca^{2+}]_i$ increases and electrical activity were normal in HFD islets, and glucose-induced ATP production was likewise unperturbed (supplementary Fig. 4*B*). Collectively, these observations indicate that insulin secretion is impaired at the level of exocytosis itself. We now demonstrate that HFD β-cells have a selective suppression of exocytosis evoked by action potential–like stimulation (trains of 50-ms depolarizations). Exocytosis monitored by capacitance measurements was reduced by 70% in response to such stimulation. Interestingly, much weaker effects were obtained in response to trains of 500-ms depolarizations. We also monitored exocytosis of granules by TIRF imaging during a 1-s depolarization. Again, there was inhibition of granule exocytosis in HFD β-cells compared with control cells during the first 400 ms of depolarization. However, at later times, the rate of exocytosis was actually enhanced in the HFD β-cells compared with what was seen in the ND cells. Thus, it appears that it is the kinetics of exocytosis rather than the release competence of the granules that is affected by high-fat feeding.

Ion channels are modulated by FFA application (24,30–32). Whole-cell K_{ATP} voltage–gated Ca^{2+} currents were not affected by the HFD. The delayed-rectifier K^+ current (K_{DR}), which is responsible for the repolarization of the Ca^{2+}-induced action potential in mouse β-cells, has been shown to be modulated upon application of FFA (24,32). A reduced K_{DR} current would be expected to prolong the action potential. It has been reported that the K_{DR} current reduction is a GPR40-dependent process (24). Overexpression of GPR40 protects mice against the diabetogenic action of HFD (33). It is possible that the latter effect is mediated by the marked prolongation of the action potential that protects the β-cell against the inhibitory effects on insulin secretion produced by Ca^{2+} channel dispersion. However, we observed no differences in the

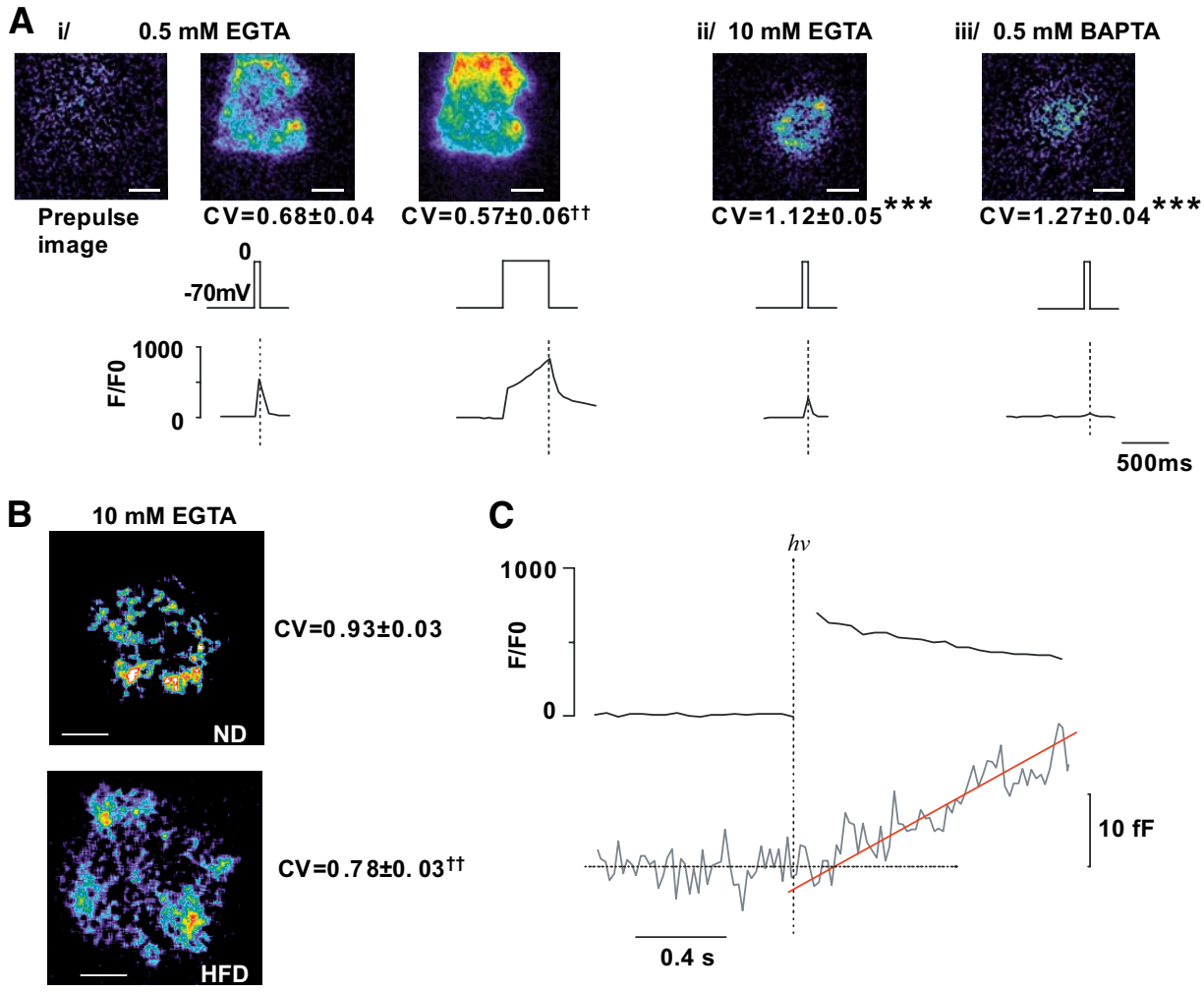

FIG. 8. HFD causes dispersion of Ca^{2+} entry. *A*: Evanescent-field illumination of voltage-clamped cells infused with 0.5 mmol/l EGTA (*i*), 10 mmol/l EGTA (*ii*), or 0.5 mmol/l BAPTA (*iii*) and Ca^{2+} Green 6F (10 μmol/l). The images in *Ai* show the prestimulatory fluorescence and the increase produced by 50- and 500-ms depolarizations, respectively. Numbers below images are CV values for the Ca^{2+} signal (mean values ± SEM) for 6 (*i*), 11 (*ii*), and 11 (*iii*) different cells. ***$P < 5 \times 10^{-5}$ (unpaired *t* test) or ††$P < 0.005$ (paired *t* test) for comparisons with CV measured after a 50-ms depolarization with 0.5 mmol/l EGTA. Scale bars: 2 μm. The vertical lines superimposed on the $[Ca^{2+}]_i$ traces indicate the end of the depolarization. *B*: As in *Aii* but using ND or HFD β-cells (as indicated). CV values for the Ca^{2+} signal during a 50-ms depolarization to 0 mV for control ($n = 12$ from three mice) and HFD ($n = 15$ from three mice) β-cells are shown to the right of each image alongside. ††$P < 0.001$ for comparison between HFD and ND β-cells. *C*: Immediate increases in $[Ca^{2+}]_i$ and delayed increase in membrane capacitance (ΔC_m) in β-cells from C57BL6J mice in response to photoliberation of caged Ca^{2+} (Ca^{2+}-np-EGTA preloaded into the cell). The trace is the average response recorded in seven cells from three different animals. The continuous red line represents the back-extrapolation toward the baseline (dashed horizontal line). The intersection of the two lines was taken as the delay. (A high-quality digital representation of this figure is available in the online issue.)

duration and upstroke or downstroke velocities of the action potentials recorded from ND and HFD β-cells (not shown).

In β-cells, exocytosis in response to brief depolarizations depends on a close association of Ca^{2+} channels and secretory granules (34). It is therefore of interest that whereas Ca^{2+} entry in ND β-cells concentrates in discrete areas, it becomes more diffuse in HFD β-cells. The effect is fairly small but this may reflect partial recovery from the in vivo effect during tissue culture. The $[Ca^{2+}]_i$ transients echoed the membrane depolarizations: no transients were observed when depolarization was +60 mV (reversal of the Ca^{2+} current), and their amplitude was unaffected by pretreatment of the cells with thapsigargin (supplementary Fig. 6). These findings suggest that the transients reflect a localized increase in $[Ca^{2+}]_i$ due to Ca^{2+} influx through individual Ca^{2+} channels, with little contribution of release from intracellular stores.

We have previously demonstrated that the β-cell Ca^{2+} channels aggregate into triplets and argued that this arrangement is a prerequisite for rapid exocytosis (22). The fact that the Ca^{2+} entry becomes dispersed in HFD β-cells is suggestive of less efficient clustering. In the HFD β-cells, Ca^{2+} still enters the β-cell during electrical activity, but the increases in $[Ca^{2+}]_i$ occur too far away from the release-competent granules to trigger their release. This accounts for the apparent reduction of the Ca^{2+} sensitivity of exocytosis (Fig. 7*B*). During longer depolarizations, however, the Ca^{2+} channels stay open long enough to allow the $[Ca^{2+}]_i$ increase to spread through the cytosol (compare 50- and 500-ms depolarizations in Fig. 8*Ai*). Under these conditions, granules situated too far away from the Ca^{2+} channels to be released during brief stimulation would be exposed to exocytotic levels of $[Ca^{2+}]_i$. In this context, it is of interest that insulin secretion evoked by high K^+ stimulation was the same in HFD and ND islets. This stimulation protocol also activates the Ca^{2+} channels long enough to allow $[Ca^{2+}]_i$ equilibration

throughout the β-cell and release any release-competent granule regardless of their proximity to the Ca^{2+} channels. The fact that high K^+ was tested in the presence of 20 mmol/l glucose also allows us to exclude an effect of HFD on the amplifying action of glucose. In this context, it may be worth pointing out that tolbutamide fails to restore insulin secretion from HFD islets to that seen in ND islets because the action potentials triggered by the sulfonylurea are of the same (brief) type as those elicited in response to glucose (35). The fact that first-phase and second-phase insulin secretions are similarly affected (Fig. 3) is perfectly consistent with these observations. Both first- and second-phase insulin secretion is triggered by action potential firing (36). First-phase secretion is larger because it coincides with a brief period of continuous action potential firing, whereas action potentials are grouped in bursts at steady state (Fig. 6). Another factor that contributes to the prominence of first-phase insulin secretion is the number of readily releasable pool (RRP) granules. It is likely that RRP is larger to begin with and that the rate of secretion will decline simply because there are fewer granules for Ca^{2+} entering the cell to act on. The concept that short-lived localized increases in $[Ca^{2+}]_i$ trigger exocytosis may seem difficult to reconcile with the finding that few granules undergo exocytosis during the initial 100–200 ms. In β-cells from NMRI mice, we have observed a delay between photorelease of caged Ca^{2+} (to produce a uniform step increase in $[Ca^{2+}]_i$) and the initiation of exocytosis of only 10 ms (22). In this study, based on β-cells from C57BL6J mice, the latency was >200 ms. These observations suggest that (for reasons that remain to be clarified) there is a significant delay between the triggering and initiation of exocytosis.

Why is there a selective inhibition of exocytosis evoked by rapid depolarizations in HFD islets? The effects of high-fat feeding on exocytosis are reminiscent of those recently found to occur after reduced expression of *Tcf7l2* (37). However, no changes in *Tcf7l2* expression could be detected (supplementary Table 1). We also failed to detect any major changes in the expression of 16 genes encoding key exocytotic proteins. In this context, it is of great interest that the microRNA miR34a becomes upregulated in rodent β-cells exposed to palmitate (38). However, the fact that insulin secretion evoked by high K^+ and exocytosis in response to long depolarizations was similar in HFD and ND β-cells militates against any major defects in β-cell exocytosis. Rather, dispersion of Ca^{2+} entry is likely to be key to understanding the mechanisms leading to impaired insulin secretion from HFD islets. Results obtained in isolated islets exposed to the free fatty acid palmitate for >72 h are very similar to those described here (16). The present data extend these observations by providing a direct link between increased dietary lipids and impaired β-cell function. In mice fed the HFD, there is a 20-fold increase in pancreatic triglycerides (16). Increased adipocyte content of the pancreas will result in increased flux of FFAs in the extracellular space, some of which will be adjacent to the pancreatic islets (16), and thereby suppress insulin secretion by the mechanism that we have previously documented in vitro (16). If these data can be extended to humans, they may have both dietary and therapeutic implications.

ACKNOWLEDGMENTS

D.G. holds a Wellcome Trust Senior Fellowship in basic biomedical science (057733). F.A. was supported by a CNPq fellowship from Brazil. This work was supported by the Wellcome Trust, the European Union (Eurodia), and Diabetes U.K.

No potential conflicts of interest relevant to this article were reported.

We thank Alice Rothwell, Ann Stanmore, and David Wiggins for technical assistance.

REFERENCES

1. Lillioja S, Mott DM, Spraul M, Ferraro R, Foley JE, Ravussin E, Knowler WC, Bennett PH, Bogardus C. Insulin resistance and insulin secretory dysfunction as precursors of non-insulin-dependent diabetes mellitus: prospective studies of Pima Indians. N Engl J Med 1993;329:1988–1992
2. Colditz GA, Willett WC, Stampfer MJ, Manson JE, Hennekens CH, Arky RA, Speizer FE. Weight as a risk factor for clinical diabetes in women. Am J Epidemiol 1990;132:501–513
3. Kashyap S, Belfort R, Gastaldelli A, Pratipanawatr T, Berria R, Pratipanawatr W, Bajaj M, Mandarino L, DeFronzo R, Cusi K. A sustained increase in plasma free fatty acids impairs insulin secretion in nondiabetic subjects genetically predisposed to develop type 2 diabetes. Diabetes 2003;52:2461–2474
4. Buettner R, Scholmerich J, Bollheimer LC. High-fat diets: modeling the metabolic disorders of human obesity in rodents. Obesity (Silver Spring) 2007;15:798–808
5. Kaku K, Fiedorek FT Jr, Province M, Permutt MA. Genetic analysis of glucose tolerance in inbred mouse strains: evidence for polygenic control. Diabetes 1988;37:707–713
6. Kooptiwut S, Zraika S, Thorburn AW, Dunlop ME, Darwiche R, Kay TW, Proietto J, Andrikopoulos S. Comparison of insulin secretory function in two mouse models with different susceptibility to beta-cell failure. Endocrinology 2002;143:2085–2092
7. Fearnside JF, Dumas ME, Rothwell AR, Wilder SP, Cloarec O, Toye A, Blancher C, Holmes E, Tatoud R, Barton RH, Scott J, Nicholson JK, Gauguier D. Phylometabonomic patterns of adaptation to high fat diet feeding in inbred mice. PLoS ONE 2008;3:e1668
8. Zhou YP, Grill VE. Long-term exposure of rat pancreatic islets to fatty acids inhibits glucose-induced insulin secretion and biosynthesis through a glucose fatty acid cycle. J Clin Invest 1994;93:870–876
9. Crespin SR, Greenough WB III, Steinberg D. Stimulation of insulin secretion by infusion of free fatty acids. J Clin Invest 1969;48:1934–1943
10. Olofsson CS, Salehi A, Holm C, Rorsman P. Palmitate increases L-type Ca2+ currents and the size of the readily releasable granule pool in mouse pancreatic beta-cells. J Physiol 2004;557:935–948
11. Olofsson CS, Collins S, Bengtsson M, Eliasson L, Salehi A, Shimomura K, Tarasov A, Holm C, Ashcroft F, Rorsman P. Long-term exposure to glucose and lipids inhibits glucose-induced insulin secretion downstream of granule fusion with plasma membrane. Diabetes 2007;56:1888–1897
12. Toye AA, Lippiat JD, Proks P, Shimomura K, Bentley L, Hugill A, Mijat V, Goldsworthy M, Moir L, Haynes A, Quarterman J, Freeman HC, Ashcroft FM, Cox RD. A genetic and physiological study of impaired glucose homeostasis control in C57BL/6J mice. Diabetologia 2005;48:675–686
13. Bonnevie-Nielsen V, Steffes MW, Lernmark A. A major loss in islet mass and B-cell function precedes hyperglycemia in mice given multiple low doses of streptozotocin. Diabetes 1981;30:424–429
14. Göpel SO, Kanno T, Barg S, Eliasson L, Galvanovskis J, Renström E, Rorsman P. Activation of Ca(2+)-dependent K(+) channels contributes to rhythmic firing of action potentials in mouse pancreatic beta cells. J Gen Physiol 1999;114:759–770
15. Olofsson CS, Salehi A, Göpel SO, Holm C, Rorsman P. Palmitate stimulation of glucagon secretion in mouse pancreatic alpha-cells results from activation of L-type calcium channels and elevation of cytoplasmic calcium. Diabetes 2004;53:2836–2843
16. Hoppa MB, Collins S, Ramracheya R, Hodson L, Amisten S, Zhang Q, Johnson P, Ashcroft FM, Rorsman P. Chronic palmitate exposure inhibits insulin secretion by dissociation of Ca(2+) channels from secretory granules. Cell Metab 2009;10:455–465
17. Barg S, Olofsson CS, Schriever-Abeln J, Wendt A, Gebre-Medhin S, Renström E, Rorsman P. Delay between fusion pore opening and peptide release from large dense-core vesicles in neuroendocrine cells. Neuron 2002;33:287–299
18. Nunemaker CS, Zhang M, Wasserman DH, McGuinness OP, Powers AC,

Bertram R, Sherman A, Satin LS. Individual mice can be distinguished by the period of their islet calcium oscillations: is there an intrinsic islet period that is imprinted in vivo? Diabetes 2005;54:3517–3522
19. Rorsman P, Renström E. Insulin granule dynamics in pancreatic beta cells. Diabetologia 2003;46:1029–1045
20. Olofsson CS, Göpel SO, Barg S, Galvanovskis J, Ma X, Salehi A, Rorsman P, Eliasson L. Fast insulin secretion reflects exocytosis of docked granules in mouse pancreatic B-cells. Pflugers Arch 2002;444:43–51
21. Shibasaki T, Takahashi H, Miki T, Sunaga Y, Matsumura K, Yamanaka M, Zhang C, Tamamoto A, Satoh T, Miyazaki J, Seino S. Essential role of Epac2/Rap1 signaling in regulation of insulin granule dynamics by cAMP. Proc Natl Acad Sci U S A 2007;104:19333–19338
22. Barg S, Ma X, Eliasson L, Galvanovskis J, Göpel SO, Obermüller S, Platzer J, Renström E, Trus M, Atlas D, Striessnig J, Rorsman P. Fast exocytosis with few Ca(2+) channels in insulin-secreting mouse pancreatic B cells. Biophys J 2001;81:3308–3323
23. Ahrén B, Gudbjartsson T, Al-Amin AN, Mårtensson H, Myrsén-Axcrona U, Karlsson S, Mulder H, Sundler F. Islet perturbations in rats fed a high-fat diet. Pancreas 1999;18:75–83
24. Feng DD, Luo Z, Roh SG, Hernandez M, Tawadros N, Keating DJ, Chen C. Reduction in voltage-gated K+ currents in primary cultured rat pancreatic beta cells by linoleic acids. Endocrinology 2006;147:674–682
25. Reimer MK, Ahrén B. Altered beta-cell distribution of pdx-1 and GLUT-2 after a short-term challenge with a high-fat diet in C57BL/6J mice. Diabetes 2002;51:S138–S143
26. Qiu L, List EO, Kopchick JJ. Differentially expressed proteins in the pancreas of diet-induced diabetic mice. Mol Cell Proteomics 2005;4:1311–1318
27. Sone H, Kagawa Y. Pancreatic beta cell senescence contributes to the pathogenesis of type 2 diabetes in high-fat diet-induced diabetic mice. Diabetologia 2005;48:58–67
28. Ahrén B, Simonsson E, Scheurink AJ, Mulder H, Myrsén U, Sundler F. Dissociated insulinotropic sensitivity to glucose and carbachol in high-fat diet-induced insulin resistance in C57BL/6J mice. Metabolism 1997;46:97–106
29. Ahrén B, Pacini G. Insufficient islet compensation to insulin resistance vs. reduced glucose effectiveness in glucose-intolerant mice. Am J Physiol Endocrinol Metab 2002;283:E738–E744
30. Feng DD, Zhao YF, Luo ZQ, Keating DJ, Chen C. Linoleic acid induces Ca2+-induced inactivation of voltage-dependent Ca2+ currents in rat pancreatic beta-cells. J Endocrinol 2008;196:377–384
31. Zhao YF, Pei J, Chen C. Activation of ATP-sensitive potassium channels in rat pancreatic beta-cells by linoleic acid through both intracellular metabolites and membrane receptor signalling pathway. J Endocrinol 2008;198:533–540
32. Jacobson DA, Weber CR, Bao S, Turk J, Philipson LH. Modulation of the pancreatic islet beta-cell-delayed rectifier potassium channel Kv2.1 by the polyunsaturated fatty acid arachidonate. J Biol Chem 2007;282:7442–7449
33. Nagasumi K, Esaki R, Iwachidow K, Yasuhara Y, Ogi K, Tanaka H, Nakata M, Yano T, Shimakawa K, Taketomi S, Takeuchi K, Odaka H, Kaisho Y. Overexpression of GPR40 in pancreatic beta-cells augments glucose-stimulated insulin secretion and improves glucose tolerance in normal and diabetic mice. Diabetes 2009;58:1067–1076
34. Barg S, Eliasson L, Renstrom E, Rorsman P. A subset of 50 secretory granules in close contact with L-type Ca2+ channels accounts for first-phase insulin secretion in mouse beta-cells. Diabetes 2002;51(Suppl. 1):S74–S82
35. Henquin JC, Meissner HP. Opposite effects of tolbutamide and diazoxide on 86Rb+ fluxes and membrane potential in pancreatic B cells. Biochem Pharmacol 1982;31:1407–1415
36. Henquin JC. Regulation of insulin secretion: a matter of phase control and amplitude modulation. Diabetologia 2009;52:739–751
37. da Silva Xavier G, Loder MK, McDonald A, Tarasov AI, Carzaniga R, Kronenberger K, Barg S, Rutter GA. TCF7L2 regulates late events in insulin secretion from pancreatic islet {beta}-cells. Diabetes 2009;58:894–905
38. Lovis P, Roggli E, Laybutt DR, Gattesco S, Yang JY, Widmann C, Abderrahmani A, Regazzi R. Alterations in microRNA expression contribute to fatty acid-induced pancreatic beta-cell dysfunction. Diabetes 2008;57:2728–2736